PHYSICAL REVIEW B **102**, 195127 (2020)

First-principles method for x-ray Thomson scattering including both elastic and inelastic features in warm dense matter

Chongjie Mo,[1,2] Zhen-Guo Fu,[3] Ping Zhang,[2,3,*] Wei Kang,[2,†] Weiyan Zhang,[2,4] and X. T. He[2,3]
[1] *Beijing Computational Science Research Center, Beijing 100193, China*
[2] *HEDPS, Center for Applied Physics and Technology, and College of Engineering, Peking University, Beijing 100871, China*
[3] *Institute of Applied Physics and Computational Mathematics, Beijing 100088, China*
[4] *China Academy of Engineering Physics, Mianyang 621900, China*

(Received 4 August 2020; revised 15 October 2020; accepted 3 November 2020; published 16 November 2020)

We show that the entire x-ray Thomson scattering (XRTS) spectrum, including both elastic and inelastic features, can be calculated from first principles in the framework of quantum perturbation theories. Our derivation shows that the elastic scattering feature in a warm dense regime is different from that of condensed matter at low temperature. In addition to the contribution from spatial fluctuations of electronic density, which dominates elastic scattering at low temperature, there is an extra contribution from partially occupied inner-shell states, which is important in the warm dense regime. Calculated XRTS of isochorically heated beryllium agrees well with previous experimental measurements, which may give this method a further edge on interpreting XRTS spectra compared to empirical modeling methods.

DOI: 10.1103/PhysRevB.102.195127

I. INTRODUCTION

Warm dense matter (WDM) has attracted much attention recently in the fields of inertial confinement fusion [1–5], planetary physics [6], and laboratory astrophysics [7]. In order to explore the unique physical properties of WDM, a series of diagnostic techniques, e.g., the streaked optical pyrometers [8,9], the x-ray absorption spectra [10–13], and, in parallel, the x-ray Thomson scattering (XRTS) methods [14], have been developed to detect temperature, density, and ionization degree of WDM in laboratory. However, the challenge to a highly accurate diagnosis of these parameters not only lies in the experimental techniques, but also in the theoretical modeling which is greatly limited by the inexplicitly revealed physical properties in a warm dense regime. The XRTS method is a typical example, whose parameter-prediction capability essentially relies on the spectrum matching between experimental measurement and theoretical prediction.

Due to the completion of advanced facilities such as x-ray free-electron lasers [15] and high-power lasers [16–18], the experimental conditions of XRTS are much improved. In 2009, it was first successfully used by Lee *et al.* for the diagnostics in shock compression experiments [19]. In 2015, with the x-ray free-electron lasers (XFELs) as probes, the spectral resolution was much improved [20]. However, the associated theoretical description is still under development. The most commonly used model of XRTS was proposed by Chihara for the first time [21,22] and then straightforwardly applied to scattering experiments [23,24]. Its spectrum intensity is directly related to the system's electronic dynamic structure factor (DSF) [25,26]. The Chihara decomposition has its advantages in perspicuous physical explanations of the scattering mechanism and small computational costs as well, but there are still issues that are not well resolved even with additional corrections [14,27–31], e.g., the division of bound and free electrons, the inhomogeneous background of ionic potential, etc.

Recently, several works based on first-principles methods have been reported to address different aspects of XRTS modeling, concerning the ionic feature [32–34], the free-free contribution [35–38], and the bound-free transitions [39]. Particularly, the time-dependent density functional theory (TDDFT) was found to be very useful to predict the inelastic feature of XRTS spectra, which was first introduced by Baczewski *et al.* in a real-time form [39] and then followed by the implementation of a perturbation formula by Mo *et al.* [35]. Compared with empirical methods, first-principles approaches avoid the unnecessary division of free and bound electrons, and include the majority of electron-electron and electron-ion interactions in an inhomogeneous environment. However, one may have noticed that current theoretical models are actually based on formulas of condensed-matter physics at low temperature. Whether they can be directly used to describe the XRTS of WDM remains an open question. As we shall illustrate below, some of the interesting features of warm dense states may not have been revealed in previous first-principles investigations [35,37,39–41].

In this work, we show that in the framework of quantum perturbation theories, the entire XRTS spectra, including both elastic and inelastic features, can be calculated from first principles. Our formula shows that the elastic scattering feature in a warm dense regime is different from that at low temperature, where the condensed-matter physics formula holds. In addition to the contribution from spatial fluctuations of

---

[*] zhang_ping@iapcm.ac.cn
[†] weikang@pku.edu.cn

electronic density, which dominates elastic scatterings at low temperature, there is an extra contribution from partially occupied inner-shell states, which is important in the warm dense regime. The XRTS spectra of isochorically heated beryllium (Be) thus calculated display remarkable agreement with experimental measurements [24], which may give this method a further edge in interpreting XRTS spectra compared to empirical modeling methods.

The rest of the article is organized as follows. All necessary formulas are derived in Sec. II. In Sec. III, we concisely describe the numerical details for carrying out the calculation. Numerical results of elastic and inelastic features together with a comparison with experimentally measured XRTS spectra of isochorically heated Be are presented in Sec. IV. Section V concludes the work with a short summary.

II. THEORETICAL FORMULAS

Scattering of photons by a many-electron system is usually described by the famous Kramers-Heisenberg formula, which we find is an appropriate starting point to derive the theoretical formulas of XRTS applied to WDM. Here, we focus on the derivation of the elastic feature of XRTS and the single-particle representation of the formulas used in conjugation with the first-principles molecular dynamics (FPMD) method. The atomic units together with $k_B = 1$ will be used in the formulas hereinafter.

A. Kramers-Heisenberg formula

We start from a nonrelativistic Hamiltonian,

$$\hat{\mathcal{H}} = \sum_j \frac{1}{2}[\boldsymbol{P}_j - \boldsymbol{A}(\boldsymbol{r}_j, t)]^2 + \sum_{j<j'} V(|\boldsymbol{r}_j - \boldsymbol{r}'_j|) + \sum_j \phi(\boldsymbol{r}_j) + \sum_{\boldsymbol{k}\lambda} \omega_{\boldsymbol{k}} \left[\hat{a}^{\dagger}_{\boldsymbol{k}\lambda}\hat{a}_{\boldsymbol{k}\lambda} + \frac{1}{2}\right], \tag{1}$$

consisting of electrons and quantized x-ray photons. Here, $\boldsymbol{r}_j$ is the position of the jth electron, $\boldsymbol{P}_j = -i\partial/\partial\boldsymbol{r}_j$ is the corresponding momentum operator of the electron, V is the interaction between electrons, and ϕ is the Coulomb potential provided by ions in the system, which move much more slowly than electrons and are therefore treated as static during the scattering. X-ray photons are represented by their wave vector $\boldsymbol{k}$, polarization λ, and frequency $\omega_{\boldsymbol{k}}$, together with the creation and annihilation operators $\hat{a}^{\dagger}_{\boldsymbol{k}\lambda}$ and $\hat{a}_{\boldsymbol{k}\lambda}$. $\boldsymbol{A}(\boldsymbol{r}, t)$ is the vector potential of x-ray photons, which can be expressed as a linear superposition of plane waves as

$$\boldsymbol{A}(\boldsymbol{r}, t) = \sum_{\boldsymbol{k}\lambda} \sqrt{\frac{2\pi}{V\omega_{\boldsymbol{k}}}} \{\boldsymbol{\epsilon}_{\boldsymbol{k}\lambda}\hat{a}_{\boldsymbol{k}\lambda} \exp[i(\boldsymbol{k}\cdot\boldsymbol{r} - \omega_{\boldsymbol{k}}t)] + \boldsymbol{\epsilon}^*_{\boldsymbol{k}\lambda}\hat{a}^{\dagger}_{\boldsymbol{k}\lambda} \exp[-i(\boldsymbol{k}\cdot\boldsymbol{r} - \omega_{\boldsymbol{k}}t)]\}, \tag{2}$$

where V is the normalization volume, and $\boldsymbol{\epsilon}_{\boldsymbol{k}\lambda}$ is the complex polarization unit vector including a phase factor.

The interaction $\hat{\mathcal{H}}'(t)$ between x-ray photons and electrons can be divided into

$$\hat{\mathcal{H}}'(t) = \hat{\mathcal{H}}'_1(t) + \hat{\mathcal{H}}'_2(t), \tag{3}$$

with

$$\hat{\mathcal{H}}'_1(t) = \sum_j \frac{1}{2}|\boldsymbol{A}(\boldsymbol{r}_j, t)|^2,$$

$$\hat{\mathcal{H}}'_2(t) = -\sum_j \frac{1}{2}[\boldsymbol{P}_j \cdot \boldsymbol{A}(\boldsymbol{r}_j, t) + \boldsymbol{A}(\boldsymbol{r}_j, t) \cdot \boldsymbol{P}_j]. \tag{4}$$

We note that direct scattering of x-ray photons by ions is neglected in the Hamiltonian since the scattering cross section is inversely proportional to the square of the mass of scattering particles, which makes the scattering amplitude of ions six orders smaller than that of electrons [25]. Electronic spins, which give rise to magnetic scatterings, are not considered either because their effects are blurred by thermal fluctuations under warm dense conditions.

In perturbation treatments, the initial state $|I\rangle$ and the final state $|F\rangle$ may be formally expressed as direct products of a photonic state and an electronic state as $|I\rangle = |\tilde{p}_1\rangle \otimes |\boldsymbol{\alpha}\rangle$ and $|F\rangle = |\tilde{p}_2\rangle \otimes |\boldsymbol{\beta}\rangle$, where $|\tilde{p}_1\rangle$ and $|\tilde{p}_2\rangle$ are many-body x-ray photonic states, while $|\boldsymbol{\alpha}\rangle$ and $|\boldsymbol{\beta}\rangle$ are many-body electronic states. Here, $|I\rangle$ and $|F\rangle$ are considered as *exact* states of the total Hamiltonian $\hat{\mathcal{H}}$ in Eq. (1). $|\boldsymbol{\alpha}\rangle$ and $|\boldsymbol{\beta}\rangle$ are therefore, in general, different from the energy states of the nonperturbed electronic system without the incidence of x-ray photons [42].

Transition rate $w_{I\to F}$, accurate to the second order of $\boldsymbol{A}(\boldsymbol{r}, t)$, can then be derived from Fermi's golden rule as

$$w_{I\to F} = 2\pi \left| \langle F|\hat{\mathcal{H}}'_1|I\rangle + \sum_N \frac{\langle F|\hat{\mathcal{H}}'_2|N\rangle\langle N|\hat{\mathcal{H}}'_2|I\rangle}{E_I - E_N} \right|^2 \delta(E_I - E_F), \tag{5}$$

with $|N\rangle$ an intermediate state. For a given transition from the $(\omega_1, k_1, \boldsymbol{\epsilon}_1)$ state to the $(\omega_2, k_2, \boldsymbol{\epsilon}_2)$ state, the transition rate can be further expanded as

$$w_{I\to F} = \frac{8\pi^3 N_1(N_2+1)}{V^2\omega_1\omega_2} \left| \boldsymbol{\epsilon}_1 \cdot \boldsymbol{\epsilon}^*_2 \langle\boldsymbol{\beta}| \sum_j e^{i(\boldsymbol{k}_1-\boldsymbol{k}_2)\cdot\boldsymbol{r}_j} |\boldsymbol{\alpha}\rangle + \sum_{\boldsymbol{\gamma}} \sum_{jj'} \left[\frac{\langle\boldsymbol{\beta}|e^{-i\boldsymbol{k}_2\cdot\boldsymbol{r}_j}\boldsymbol{\epsilon}^*_2 \cdot \boldsymbol{P}_j|\boldsymbol{\gamma}\rangle\langle\boldsymbol{\gamma}|e^{i\boldsymbol{k}_1\cdot\boldsymbol{r}_{j'}}\boldsymbol{\epsilon}_1 \cdot \boldsymbol{P}_{j'}|\boldsymbol{\alpha}\rangle}{E_{\boldsymbol{\alpha}} - E_{\boldsymbol{\gamma}} + \omega_1} + \frac{\langle\boldsymbol{\beta}|e^{i\boldsymbol{k}_1\cdot\boldsymbol{r}_j}\boldsymbol{\epsilon}_1 \cdot \boldsymbol{P}_j|\boldsymbol{\gamma}\rangle\langle\boldsymbol{\gamma}|e^{-i\boldsymbol{k}_2\cdot\boldsymbol{r}_{j'}}\boldsymbol{\epsilon}^*_2 \cdot \boldsymbol{P}_{j'}|\boldsymbol{\alpha}\rangle}{E_{\boldsymbol{\alpha}} - E_{\boldsymbol{\gamma}} - \omega_2} \right] \right|^2 \delta(E_{\boldsymbol{\alpha}} - E_{\boldsymbol{\beta}} + \omega_1 - \omega_2), \tag{6}$$

where N_1 and N_2 are photon numbers associated with the photon transition, and $|\boldsymbol{\gamma}\rangle$ is an intermediate many-body electronic state similar to $|\boldsymbol{\alpha}\rangle$ and $|\boldsymbol{\beta}\rangle$. The Kramers-Heisenberg formula for the differential scattering cross section is then given by

$$\left(\frac{d^2\sigma}{d\Omega_2 d\omega_2}\right)_{I\to F} = w_{I\to F}\times\frac{V\omega_2^2}{8\pi^3 c^3}\times\left(\frac{N_1 c}{V}\right)^{-1}, \tag{7}$$

where c is the light speed, $(\omega_2^2 V)/(8\pi^3 c^3)$ is the density of the final photon state, and $N_1 c/V$ is the incident flux.

B. Decomposition of dynamic structure factor

For the scattering of x-ray photons, the Kramers-Heisenberg formula given by Eq. (7) can be much simplified. First, the energies of x-ray photons are of the order of several-thousand electron volts, so that the second term inside the modulus in Eq. (6) can be neglected if one considers the Raman-like process as a less significant feature. Second, under x-ray scattering conditions, $\omega_1 \approx \omega_2$, and $N_2 = 0$ since there are no scattered photons before the scattering happens. With all these simplifications, the total scattering cross section can be written in the form

$$\frac{d^2\sigma}{d\Omega_2 d\omega_2} = \sigma_{\mathrm{Th}} S(\boldsymbol{q},\omega), \tag{8}$$

where σ_{Th} is the classical Thomson scattering cross section defined as $\sigma_{\mathrm{Th}} \equiv |\boldsymbol{\epsilon}_1\cdot\boldsymbol{\epsilon}_2^*|^2/c^4$, $\omega = \omega_1 - \omega_2$ is the energy difference between the incident and scattered x-ray photons, $\boldsymbol{q} = \boldsymbol{k}_1 - \boldsymbol{k}_2$ is the momentum difference, and $S(\boldsymbol{q},\omega)$ is the electronic DSF. It is obtained from the average of the cross section for all pairs of transitions as

$$S(\boldsymbol{q},\omega) = \left\langle \sum_{\boldsymbol{\alpha\beta}} g_{\boldsymbol{\alpha}} \left| \langle\boldsymbol{\beta}|\sum_j e^{i\boldsymbol{q}\cdot\boldsymbol{r}_j}|\boldsymbol{\alpha}\rangle \right|^2 \delta(E_{\boldsymbol{\alpha}} - E_{\boldsymbol{\beta}} + \omega)\right\rangle. \tag{9}$$

The average process in Eq. (9) is explicitly split into two steps with the help of the Born-Oppenheimer approximation. The first step is the average of all initial and final many-body electronic eigenstates $|\boldsymbol{\alpha}\rangle$ and $|\boldsymbol{\beta}\rangle$ for a given ionic configuration. The initial state $|\boldsymbol{\alpha}\rangle$ has a weight $g_{\boldsymbol{\alpha}} = Z^{-1}\exp(-E_{\boldsymbol{\alpha}}/T)$ in the average, if electrons are assumed in equilibrium with each other at temperature T. Z is the partition function of the electrons. The second step is the average of all possible ionic configurations, represented by the outermost $\langle\cdot\rangle$ in Eq. (9). Note that electrons are not required in equilibrium with ions, in general, for the application of Eq. (9), so that it can also be applied to nonequilibrium situations, e.g., x-ray scatterings in warm dense metal isochorically heated by femtosecond free-electron lasers [15], where the motion of ions is neglected and electrons are considered heated to a temperature of several electron volts [43–45]. This process is subtly different from the treatment of Vorberger and Chapman [46] in the coupling between ions and electrons.

The many-body electronic states $|\boldsymbol{\alpha}\rangle$ and $|\boldsymbol{\beta}\rangle$ can be further approximated using noninteracting (Hartree-like) electron approximation [47], where electrons are viewed as noninteracting particles in an effective potential. It yields a complete set of orthonormal single-particle energy eigenstates, denoted as $|n\rangle$ hereinafter, and the energy is ε_n accordingly. Using this set of single-particle states, the operator in Eq. (9) can be written in the form of creation operator $\hat{c}_n^\dagger$ and annihilation operator $\hat{c}_n$ as

$$\sum_j e^{-i\boldsymbol{q}\cdot\boldsymbol{r}_j} = \sum_{nm}\langle n|e^{-i\boldsymbol{q}\cdot\boldsymbol{r}}|m\rangle \hat{c}_n^\dagger \hat{c}_m, \tag{10}$$

where

$$\langle n|e^{-i\boldsymbol{q}\cdot\boldsymbol{r}}|m\rangle = \int d\boldsymbol{r} e^{-i\boldsymbol{q}\cdot\boldsymbol{r}}\varphi_n^*(\boldsymbol{r})\varphi_m(\boldsymbol{r}), \tag{11}$$

$\boldsymbol{r}$ is the coordinates of the particle, and $\varphi_m(\boldsymbol{r})$ is the mth single-particle wave function. The $S(\boldsymbol{q},\omega)$ of electrons is now expressed as

$$\begin{aligned} S(\boldsymbol{q},\omega) = \Bigg\langle & \sum_{\boldsymbol{\alpha\beta}}\sum_{mnkj} g_{\boldsymbol{\alpha}}\langle\boldsymbol{\alpha}|\hat{c}_n^\dagger\hat{c}_m|\boldsymbol{\beta}\rangle\langle\boldsymbol{\beta}|\hat{c}_j^\dagger\hat{c}_k|\boldsymbol{\alpha}\rangle \\ & \times \langle n|e^{-i\boldsymbol{q}\cdot\boldsymbol{r}}|m\rangle\langle j|e^{i\boldsymbol{q}\cdot\boldsymbol{r}}|k\rangle\delta(E_{\boldsymbol{\alpha}} - E_{\boldsymbol{\beta}} + \omega)\Bigg\rangle. \end{aligned} \tag{12}$$

The summation in Eq. (12) with respect to m and n can be explicitly separated into a diagonal part $S_1(\boldsymbol{q},\omega)$ and a nondiagonal part $S_2(\boldsymbol{q},\omega)$ according to whether m equals n. For the diagonal part where $m = n$, $\hat{c}_n^\dagger\hat{c}_n$ is just the number operator $\hat{N}_n$ of the nth single-particle state, which is nonzero only if $|\boldsymbol{\alpha}\rangle = |\boldsymbol{\beta}\rangle$. $S_1(\boldsymbol{q},\omega)$ is then reduced to

$$\begin{aligned} S_1(\boldsymbol{q},\omega) = \Bigg\langle & \sum_{nk}\sum_{\boldsymbol{\alpha}} g_{\boldsymbol{\alpha}}\langle\boldsymbol{\alpha}|\hat{N}_n|\boldsymbol{\alpha}\rangle\langle\boldsymbol{\alpha}|\hat{N}_k|\boldsymbol{\alpha}\rangle \\ & \times \langle n|e^{-i\boldsymbol{q}\cdot\boldsymbol{r}}|n\rangle\langle k|e^{i\boldsymbol{q}\cdot\boldsymbol{r}}|k\rangle\Bigg\rangle\delta(\omega). \end{aligned} \tag{13}$$

It can further be divided into two parts according to whether or not n equals k. For the part where $n = k$, one has

$$S_1'(\boldsymbol{q},\omega) = \left\langle\sum_n f_n|\langle n|e^{-i\boldsymbol{q}\cdot\boldsymbol{r}}|n\rangle|^2\right\rangle\delta(\omega), \tag{14}$$

where $f_n = 1/\exp[(\varepsilon_n - \mu)/T] + 1$, and μ is the chemical potential of the electron system. Equation (14) can be derived if one notices that $\langle\boldsymbol{\alpha}|\hat{N}_n|\boldsymbol{\alpha}\rangle^2 = \langle\boldsymbol{\alpha}|\hat{N}_n|\boldsymbol{\alpha}\rangle$, which equals one if the nth single-particle state is occupied, and zero otherwise. Averaging all possible many-body states $|\boldsymbol{\alpha}\rangle$ then gives $\sum_{\boldsymbol{\alpha}} g_{\boldsymbol{\alpha}}\langle\boldsymbol{\alpha}|\hat{N}_n|\boldsymbol{\alpha}\rangle = f_n$.

The average $\sum_{\boldsymbol{\alpha}} g_{\boldsymbol{\alpha}}\langle\boldsymbol{\alpha}|\hat{N}_n|\boldsymbol{\alpha}\rangle\langle\boldsymbol{\alpha}|\hat{N}_k|\boldsymbol{\alpha}\rangle$ for $n \neq k$ is just $f_n f_k$, since the occupation of the nth and the kth single-particle states in each $|\boldsymbol{\alpha}\rangle$ is independent. The $n \neq k$ part in Eq. (13) is then

$$S_1''(\boldsymbol{q},\omega) = \left\langle\sum_{n\neq k} f_n f_k\langle n|e^{-i\boldsymbol{q}\cdot\boldsymbol{r}}|n\rangle\langle k|e^{i\boldsymbol{q}\cdot\boldsymbol{r}}|k\rangle\right\rangle\delta(\omega). \tag{15}$$

It can be further rewritten as

$$S_1''(\boldsymbol{q},\omega) = \left\langle|\overline{\rho(\boldsymbol{q})}|^2 - \sum_n f_n^2|\langle n|e^{-i\boldsymbol{q}\cdot\boldsymbol{r}}|n\rangle|^2\right\rangle\delta(\omega), \tag{16}$$

where $\overline{\rho(\boldsymbol{q})} = \sum_n f_n\langle n|e^{-i\boldsymbol{q}\cdot\boldsymbol{r}}|n\rangle = \int d\boldsymbol{r} e^{-i\boldsymbol{q}\cdot\boldsymbol{r}}\rho(\boldsymbol{r})$, which is just the Fourier transformation of the total electronic charge density. Combining the two parts $S_1'(\boldsymbol{q},\omega)$ and $S_1''(\boldsymbol{q},\omega)$, one arrives at an expression of $S_1(\boldsymbol{q},\omega)$ as

$$S_1(\boldsymbol{q},\omega) = S_1^a(\boldsymbol{q},\omega) + S_1^b(\boldsymbol{q},\omega), \tag{17}$$

with

$$S_1^a(\boldsymbol{q},\omega)=\langle|\overline{\rho(\boldsymbol{q})}|^2\rangle\delta(\omega), \tag{18}$$

and

$$S_1^b(\boldsymbol{q},\omega)=\left\langle\sum_n f_n(1-f_n)|\langle n|e^{-i\boldsymbol{q}\cdot\boldsymbol{r}}|n\rangle|^2\right\rangle\delta(\omega). \tag{19}$$

Now, we consider the nondiagonal part $S_2(\boldsymbol{q},\omega)$, where $n\neq m$. The nonzero terms have to satisfy the following two conditions. First, $n=k$ and $m=j$. Second, $|\boldsymbol{\alpha}\rangle=\hat{c}_n^\dagger\hat{c}_m|\boldsymbol{\beta}\rangle=\hat{c}_k^\dagger\hat{c}_j|\boldsymbol{\beta}\rangle$, which further leads to $E_{\boldsymbol{\beta}}-E_{\boldsymbol{\alpha}}=\varepsilon_n-\varepsilon_m$ or $E_{\boldsymbol{\beta}}-E_{\boldsymbol{\alpha}}=\varepsilon_k-\varepsilon_j$. Under these conditions, $S_2(\boldsymbol{q},\omega)$ becomes

$$\begin{aligned}S_2(\boldsymbol{q},\omega)=\Bigg\langle&\sum_{n\neq m}\sum_{\boldsymbol{\alpha}}g_{\boldsymbol{\alpha}}\langle\boldsymbol{\alpha}|\hat{c}_n^\dagger\hat{c}_m\hat{c}_m^\dagger\hat{c}_n|\boldsymbol{\alpha}\rangle\\&\times\langle n|e^{-i\boldsymbol{q}\cdot\boldsymbol{r}}|m\rangle\langle m|e^{i\boldsymbol{q}\cdot\boldsymbol{r}}|n\rangle\delta(\varepsilon_n-\varepsilon_m+\omega)\Bigg\rangle.\end{aligned} \tag{20}$$

Since $\hat{c}_n^\dagger\hat{c}_m\hat{c}_m^\dagger\hat{c}_n=\hat{N}_n(1-\hat{N}_m)$, the average $\sum_{\boldsymbol{\alpha}}g_{\boldsymbol{\alpha}}\langle\boldsymbol{\alpha}|\hat{c}_n^\dagger\hat{c}_m\hat{c}_m^\dagger\hat{c}_n|\boldsymbol{\alpha}\rangle$ gives a factor of $f_n(1-f_m)$. The nondiagonal part reduces to

$$S_2(\boldsymbol{q},\omega)=\left\langle\sum_{n\neq m}f_n(1-f_m)|\langle n|e^{-i\boldsymbol{q}\cdot\boldsymbol{r}}|m\rangle|^2\delta(\varepsilon_n-\varepsilon_m+\omega)\right\rangle. \tag{21}$$

C. $S_1(\boldsymbol{q},\boldsymbol{\omega})$: Elastic scattering feature

In order to understand how $S_1(\boldsymbol{q},\omega)$ varies with temperature, we first examine the dependency of $\overline{\rho(\boldsymbol{q})}=\sum_n f_n\langle n|e^{-i\boldsymbol{q}\cdot\boldsymbol{r}}|n\rangle$ on the shape of single-particle wave function $|n\rangle$. Let us consider two extreme conditions: (1) The inner core electrons, of which the spatial extension is much smaller than the wavelength of the x ray. So, its probability density can be approximately viewed as a δ function. Since $\langle n|e^{-i\boldsymbol{q}\cdot\boldsymbol{r}}|n\rangle$ is just the Fourier transformation of the probability density, its value is approximately a constant close to one. (2) The excited electrons of extremely high energy, of which the wave function is approximately a plane wave [48,49]. The value of $\langle n|e^{-i\boldsymbol{q}\cdot\boldsymbol{r}}|n\rangle$ is approximately zero for $\boldsymbol{q}\neq 0$, suggesting that highly excited electrons almost do not contribute to $S_1^a(\boldsymbol{q},\omega)$. Most of the signals of elastic scattering come from more localized electrons of low energies. With the increase of temperature, more and more electrons are excited to high-energy states, which are less localized. So, the elastic signal represented by $S_1^a(\boldsymbol{q},\omega)$ will, in general, attenuate.

We then consider the average $\langle\cdot\rangle$ of ionic configurations. There are two different application scenarios. One is the isochoric heating scenario, where the motion of ions is ignored as the pulse width of the incident x ray of the free-electron laser is of the order of tens of femtoseconds. The average of ionic configurations is then taken away. In particular, $\rho(\boldsymbol{r})$ can always be expanded into a Fourier series as $\rho(\boldsymbol{r})=\sum_{\boldsymbol{G}}\overline{\rho}_{\boldsymbol{G}}\exp(i\boldsymbol{r}\cdot\boldsymbol{G})/\Omega$ for crystalline structures, where $\boldsymbol{G}$ is the inverse lattice vector and $\overline{\rho}_{\boldsymbol{G}}$ is the Fourier series calculated from $\overline{\rho}_{\boldsymbol{G}}=\int_\Omega d\boldsymbol{r}\rho(\boldsymbol{r})\exp(-i\boldsymbol{r}\cdot\boldsymbol{G})$. Here, Ω is the volume of a primitive cell. So, if there are N_{cell} primitive cells in the system, $\overline{\rho(\boldsymbol{q})}=\int d\boldsymbol{r}e^{-i\boldsymbol{q}\cdot\boldsymbol{r}}\rho(\boldsymbol{r})$ gives $|\overline{\rho(\boldsymbol{q})}|^2=N_{\text{cell}}^2\sum_{\boldsymbol{G}}|\overline{\rho}_{\boldsymbol{G}}|^2\,\delta(\boldsymbol{q}-\boldsymbol{G})$, which is the diffraction peak observed in the x-ray scattering experiments using a free-electron laser.

In a melted system where ionic configuration is random, $\langle|\overline{\rho(\boldsymbol{q})}|^2\rangle$ is usually denoted as $N_iW(\boldsymbol{q})$, with N_i the number of ions in the system. $S_1^a(\boldsymbol{q},\omega)$ can be further written into the form

$$S_1^a(\boldsymbol{q},\omega)=N_iW(\boldsymbol{q})\delta(\omega)=N_i|N(\boldsymbol{q})|^2S_{ii}(\boldsymbol{q})\delta(\omega) \tag{22}$$

formally, where $S_{ii}(\boldsymbol{q})$ is the static ionic structure factor and $N(\boldsymbol{q})$ is the electronic form factor. When the charge distribution surrounding each ion is localized and nearly the same, Eq. (22) can be derived as follows. Suppose the charge distribution near an ion located at $\boldsymbol{R}$ is $f(\boldsymbol{r}-\boldsymbol{R})$, which leads to $\rho(\boldsymbol{r})=\sum_{\boldsymbol{R}}f(\boldsymbol{r}-\boldsymbol{R})$. It follows immediately that $\overline{\rho(\boldsymbol{q})}=f(\boldsymbol{q})\sum_{\boldsymbol{R}}e^{-i\boldsymbol{q}\cdot\boldsymbol{R}}$, where $f(\boldsymbol{q})$ is the Fourier transformation of $f(\boldsymbol{r})$. $W(\boldsymbol{q})$ can then be obtained as $W(\boldsymbol{q})=|f(\boldsymbol{q})|^2\langle\sum_{\boldsymbol{R}\boldsymbol{R}'}e^{-i\boldsymbol{q}\cdot(\boldsymbol{R}-\boldsymbol{R}')}\rangle/N_i$, where $\langle\sum_{\boldsymbol{R}\boldsymbol{R}'}e^{-i\boldsymbol{q}\cdot(\boldsymbol{R}-\boldsymbol{R}')}\rangle/N_i$ is just the definition of $S_{ii}(\boldsymbol{q})$, and $f(\boldsymbol{q})=N(\boldsymbol{q})$ is the form factor which one is familiar with in the x-ray diffraction experiments of nonmetallic liquids or amorphous materials. However, in WDM, $N(\boldsymbol{q})$ cannot be determined *a priori* without the information of $S_{ii}(\boldsymbol{q})$, as the contribution of nonlocal states cannot be neglected.

The second part of $S_1(\boldsymbol{q},\omega)$, i.e., $S_1^b(\boldsymbol{q},\omega)$ in Eq. (19), has a minor contribution at very low temperature because of the factor $f_n(1-f_n)$. Only those states near the chemical potential have significant contributions to this term and can thus be neglected safely at low temperature. However, according to the properties of $\langle n|e^{-i\boldsymbol{q}\cdot\boldsymbol{r}}|n\rangle$, this part has observable contributions at relatively high temperature when a number of core electrons are partially excited. Its contribution to elastic scattering increases with the atomic number of the component elements of the system. We note that $S_1^b(\boldsymbol{q},\omega)$ is a characteristic feature of WDM since its contribution also decreases at very high temperature when most of the core states are unoccupied.

In practice, the $S_1(\boldsymbol{q},\omega)$ is calculated using the single-particle states of the unperturbed electronic system, i.e., the electronic system without incident x-ray photons, as a further approximation. It can be easily shown that this approximation only neglects higher-order corrections to $S_1(\boldsymbol{q},\omega)$ and still has a satisfactory accuracy.

So, from a theoretical point of view, we would like to stress that the ionic feature $S_{ii}(\boldsymbol{q})$ can only be accurately determined from Eq. (22) by measuring $W(\boldsymbol{q})$ in experiments under the following conditions: (1) The measured system is at relatively low temperature so that $S_1^b(\boldsymbol{q},\omega)$ can be safely neglected. (2) The electron distribution $f(\boldsymbol{r})$ is localized around each ion so that $N(\boldsymbol{q})$ can be determined *a priori* either theoretically or experimentally. Recently, there have been efforts to determine $S_{ii}(\boldsymbol{q})$ experimentally for warm dense plasmas or hot dense plasmas [50,51]. However, the localization assumption of electron distribution no longer holds in these cases. At least part of the electrons are in spatially extended excited states, and the portion of nonlocal electrons varies with the temperature and density of the system. $N(\boldsymbol{q})$ and $S_{ii}(\boldsymbol{q})$ are thus correlated to each other. There is no way to accurately determine $N(\boldsymbol{q})$ without the information of $S_{ii}(\boldsymbol{q})$, or vice versa, given $S_1^b(\boldsymbol{q},\omega)$ is already known somehow.

The decomposition of $W(\boldsymbol{q})$ in Eq. (22) is instead useful in the numerical calculations. As we shall discuss in the following section, a direct calculation of $W(\boldsymbol{q})$ from $\langle|\overline{\rho(\boldsymbol{q})}|^2\rangle$ converges quite slowly, while $N(\boldsymbol{q})$ and $S_{ii}(\boldsymbol{q})$ can be calculated much faster separately.

D. $S_2(\boldsymbol{q},\omega)$: Inelastic scattering feature

As has been shown by Schülke [25] and others through the fluctuation-dissipation theorem [42], $S_2(\boldsymbol{q},\omega)$ is proportional to the imaginary part of the complex response function $\chi(\boldsymbol{q},\boldsymbol{q}',\omega)$, i.e.,

$$S_2(\boldsymbol{q},\omega) = -\frac{V}{\pi}\frac{1}{1-e^{-\omega/T}}\langle\chi''(\boldsymbol{q},\boldsymbol{q}',\omega)|_{\boldsymbol{q}'=\boldsymbol{q}}\rangle, \tag{23}$$

where $\chi(\boldsymbol{q},\boldsymbol{q}',\omega)$ is

$$\chi(\boldsymbol{q},\boldsymbol{q}',\omega) = \frac{1}{V}\sum_{\boldsymbol{\alpha}\neq\boldsymbol{\beta}}(g_{\boldsymbol{\alpha}} - g_{\boldsymbol{\beta}}) \times \frac{\langle\boldsymbol{\alpha}|\sum_j e^{-i\boldsymbol{q}\cdot\boldsymbol{r}_j}|\boldsymbol{\beta}\rangle\langle\boldsymbol{\beta}|\sum_k e^{i\boldsymbol{q}'\cdot\boldsymbol{r}_k}|\boldsymbol{\alpha}\rangle}{E_{\boldsymbol{\alpha}} - E_{\boldsymbol{\beta}} + \omega + i\eta}, \tag{24}$$

$\chi''(\boldsymbol{q},\boldsymbol{q}',\omega)$ is its imaginary part, and η is a positive infinitesimal number. As a result, the difficulty in calculating $S_2(\boldsymbol{q},\omega)$ moves to $\chi(\boldsymbol{q},\boldsymbol{q}',\omega)$, which can be obtained through the time-dependent density functional theory (TDDFT) method.

The screening effect of dense materials is dealt with by a Dyson-like equation [52],

$$\chi(\boldsymbol{q},\boldsymbol{q}',\omega) = \chi_0(\boldsymbol{q},\boldsymbol{q}',\omega) + \sum_{\boldsymbol{q}''\boldsymbol{q}'''}\chi_0(\boldsymbol{q},\boldsymbol{q}'',\omega)K(\boldsymbol{q}'',\boldsymbol{q}''',\omega)\chi(\boldsymbol{q}''',\boldsymbol{q}',\omega), \tag{25}$$

with χ_0 is the bare density response function and K is the many-body interaction kernel. Note that Eq. (25) is not the most general form. We actually assume a linear response relation with respect to the frequency variable [53]. The advantage of this transformation is that $\chi_0(\boldsymbol{q},\boldsymbol{q}',\omega)$ can be calculated through the states of the unperturbed electronic system, which mitigates the difficulty in determining the exact states $|\boldsymbol{\alpha}\rangle$ and $|\boldsymbol{\beta}\rangle$ when one calculates $\chi(\boldsymbol{q},\boldsymbol{q}',\omega)$ directly from Eq. (24). Using the single-particle states $|m'\rangle$ and $|n'\rangle$ of the unperturbed electronic system, $\chi_0(\boldsymbol{q},\boldsymbol{q}',\omega)$ can be expressed as

$$\chi_0(\boldsymbol{q},\boldsymbol{q}',\omega) = \frac{1}{V}\sum_{n'\neq m'}(f_{n'} - f_{m'})\frac{\langle n'|e^{-i\boldsymbol{q}\cdot\boldsymbol{r}}|m'\rangle\langle m'|e^{i\boldsymbol{q}'\cdot\boldsymbol{r}}|n'\rangle}{\omega - (\varepsilon_{m'} - \varepsilon_{n'}) + i\eta}. \tag{26}$$

$K(\boldsymbol{q},\boldsymbol{q}',\omega)$ can be further split into Coulomb contribution $v_c = 4\pi/|\boldsymbol{q}|^2$ and vertex contribution $f_{xc}(\boldsymbol{q},\boldsymbol{q}',\omega)$ as $K(\boldsymbol{q},\boldsymbol{q}',\omega) = v_c(\boldsymbol{q})\delta(\boldsymbol{q}-\boldsymbol{q}') + f_{xc}(\boldsymbol{q},\boldsymbol{q}',\omega)$. When $f_{xc}(\boldsymbol{q},\boldsymbol{q}',\omega)$ is set to be 0, $\chi(\boldsymbol{q},\boldsymbol{q}',\omega)$ is then calculated with the random-phase approximation. One can also take the exchange-correlation correction to the electronic system into consideration, and one of the simplest choices is the adiabatic local density approximation [54] to $f_{xc}(\boldsymbol{q},\boldsymbol{q}',\omega)$, where f_{xc} is considered to not depend on ω and the exchange-correlation correction only relies on the local electronic density.

III. COMPUTATIONAL DETAILS

The scattering feature of warm dense Be is used as an illustration for the method. The single-particle states of the unperturbed electronic system used in the calculation of DSF are provided using the density functional theory (DFT) method, and the finite-temperature FPMD is employed to generate ionic configurations for the ionic average at temperature lower than 9 eV. For higher temperatures, the extended FPMD (ext-FPMD) method [48] is used instead to deal with the difficulty of too many electronic states demanded by the traditional FPMD method at high temperature. The molecular dynamics and DFT calculations are carried out using a revised QUANTUM ESPRESSO package [55] with the ext-FPMD method implemented.

In the FPMD or ext-FPMD simulations, 32 Be ions are put into a cubic simulation box with $\rho = 1.85$ g/cm^3. The projector augmented-wave (PAW) method [56] is employed to represent the ion-electron interaction with a plane-wave cutoff energy of 40 Ry and a core cutoff radius $r_c = 1.4$ Bohr. All four electrons ($1s^2 2s^2$) are treated as a valence, and the Perdew-Burke-Ernzerhof (PBE) [57,58] version of the exchange-correlation functional is used. 480 electronic bands are explicitly included in the calculation, with the top 128 used to determine the effective potential energy, a parameter used in the ext-FPMD method. The Brillouin zone is sampled with the Γ point, and the calculation is carried out in a canonical (NVT) ensemble with ionic and electronic temperature kept the same. The time step of the ionic motion ranges from 0.15 to 0.7 fs depending on the temperature of the system. After the system reaches the equilibrium, ~30 000 configurations are saved for further calculations.

Instead of being directly calculated from Eq. (18), $S_1^a(\boldsymbol{q},\omega)$ and $W(\boldsymbol{q})$ are calculated from Eq. (22) through $S_{ii}(\boldsymbol{q})$ and $N(\boldsymbol{q})$, which can be calculated separately with much fewer computational costs. $S_{ii}(\boldsymbol{q})$ is calculated from the Fourier transformation of the ionic pair distribution $g(\boldsymbol{r})$ as

$$S_{ii}(\boldsymbol{q}) = 1 + n_i\int[g(\boldsymbol{r}) - 1]\exp(i\boldsymbol{q}\cdot\boldsymbol{r})d\boldsymbol{r}, \tag{27}$$

where n_i is the average number density of ions, and $g(\boldsymbol{r})$ can be directly extracted from ionic configurations obtained in the molecular dynamics simulation. Following Plagemann *et al.* [33], $N(\boldsymbol{q})$ is determined through the ionic average as

$$N(\boldsymbol{q}) = \left\langle\frac{\overline{\rho(\boldsymbol{q})}}{\rho^i(\boldsymbol{q})}\right\rangle, \tag{28}$$

where $\overline{\rho(\boldsymbol{q})}$ and $\rho^i(\boldsymbol{q})$ are spatial Fourier transformations of the electronic and ionic densities separately. With this separation, one can see that the accuracy of $S_1^a(\boldsymbol{q},\omega)$ and $W(\boldsymbol{q})$ at low $\boldsymbol{q}$ is controlled by $S_{ii}(\boldsymbol{q})$, which has to be converged with a large ensemble, while the accuracy at high $\boldsymbol{q}$ is determined by $N(\boldsymbol{q})$, which needs a superhard pseudopotential to accurately compute the electronic density of core states. $S_{ii}(\boldsymbol{q})$ can then be calculated from the FPMD or ext-FPMD method with a relatively soft pseudopotential, but with a large ensemble of ~30 000 configurations. From these configurations, one can pick much fewer snapshots, e.g., 1000 as we use in the calculation, to recalculate $\overline{\rho(\boldsymbol{q})}$ with a superhard pseudopotential. These calculations are performed using a norm-conserving

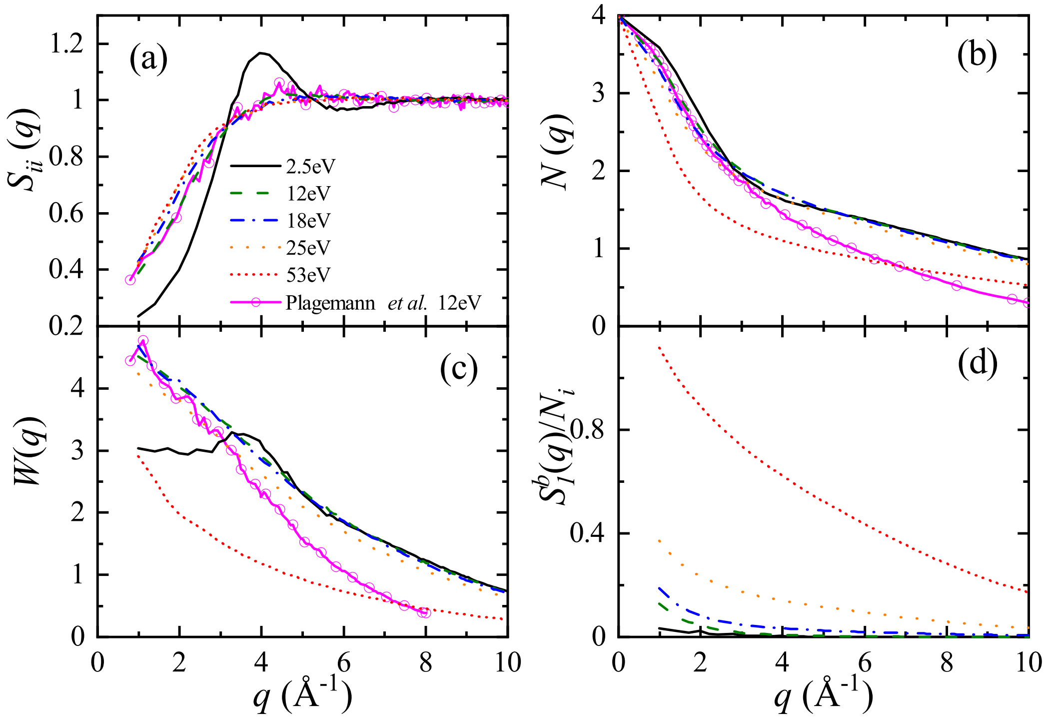

FIG. 1. Elastic features of isochorically heated Be, including (a) ionic static structure factor $S_{ii}(q)$, (b) total electronic form factor $N(q)$, (c) $W(q)$, and (d) $S_1^b(q)$ at $T = 2.5$, 12, 18, 25, and 53 eV. Numerical results of (a) $S_{ii}(q)$, (b) $N(q)$, and (c) $W(q)$ at $T = 12$ eV calculated by Plagemann *et al.* [33] are also presented as a comparison.

pseudopotential [59], with a cutoff energy of 500 Ry and $r_c = 0.4$ Bohr. $S_1^b(\boldsymbol{q})$, the static part of $S_1^b(\boldsymbol{q}, \omega)$, is also calculated in the same manner via Eq. (19). In the framework of the ext-FPMD method [48], high-energy electrons are treated as homogeneous plane waves, which have no contributions to $N(\boldsymbol{q})$ and $S_1^b(\boldsymbol{q})$ except at $\boldsymbol{q} = 0$. Moreover, all directions of $\boldsymbol{q}$ are averaged, and S_{ii}, N, W, and S_1^b are thus presented as functions of $q = |\boldsymbol{q}|$.

$\chi(\boldsymbol{q}, \omega)$ and $S_2(\boldsymbol{q}, \omega)$ are calculated using the YAMBO code [60,61]. The calculations of $\chi(\boldsymbol{q}, \omega)$ and $S_2(\boldsymbol{q}, \omega)$ are carried out at the TDDFT level with the Kohn-Sham states as the single-particle states in Eq. (26), which are recalculated with the ionic configurations generated in previous FPMD or ext-FPMD simulations. The effective ion-electron interaction is represented by a normal-conserving pseudopotential [59] with four valence electrons and an energy cutoff of 500 Ry to ensure the accuracy, and 1500 energy bands are used to ensure the convergence of the wave functions. A $2 \times 2 \times 2$ shifted k-point mesh is used to resolve the Brillouin zone.

The adiabatic local density approximation of f_{xc} is adopted in the calculation of $\chi(\boldsymbol{q}, \omega)$ following Refs. [35,62]. Finite-temperature effects on exchange-correlation interactions and f_{xc} [63,64] are not considered due to its minor effects around solid density [35,48,65]. The transferred momentum q is set to be 4.27 Å^{-1}, corresponding to a scattering angle of 125° at x-ray energy 4750 eV used in the experiment [24]. A relatively small $\eta = 0.5$ eV is adopted in Eq. (26) and the resolution of ω is 0.5 eV. The final spectra of $S_2(\boldsymbol{q}, \omega)$ presented are the average results of eight snapshots of the ionic configurations uniformly selected from the saved equilibrium ionic trajectories.

IV. RESULTS AND DISCUSSIONS

A. Elastic scattering features

With the FPMD and ext-FPMD methods, one can now calculate elastic features of XRTS at a much higher temperature than before. Figure 1 displays calculated $S_{ii}(q)$, $N(q)$, $W(q)$, and $S_1^b(q)$ of warm dense Be at temperatures reported in the XRTS experiments [24,66,67]. Figure 1(a) shows that there are no significant differences among $S_{ii}(q)$'s at $T > 10$ eV, which is a typical feature of a gaseous state. In contrast, $S_{ii}(q)$ for $T = 2.5$ eV displays the typical structure of liquids with a peak at $q = 4$ Å^{-1}. These results agree well with previous works [33,34,38,68].

$N(q)$ is a parameter closely related to x-ray diffraction experiments [69]. Figure 1(b) shows that at low temperatures, the shape of $N(q)$ is not sensitive to the variation of temperature, especially at large-q part, where $N(q)$'s almost coincide with each other. At a higher temperature ($T > 25$ eV), however, temperature becomes a determinant factor. The value of $N(q)$ becomes much smaller as a result of thermal excitations of inner-shell electrons. This temperature effect was not seriously considered before in the theoretical modeling of XRTS partly because the XRTS experiments were conducted in a relatively low-temperature regime. With the advance of experimental techniques, especially the increase of laser power, this effect becomes increasingly important.

It is also noticed that our calculated $N(q)$ at $T = 12$ eV in Fig. 1(b) displays significant differences from the one calculated by Plagemann *et al.* [33] (displayed as a solid curve with hollow circles in the figure) at large q, which further leads to a difference in $W(q)$ in Fig. 1(c). We find that the differences come from different treatments of the core electrons. In previous calculations [33], the charge density of the core electrons was directly provided by the PAW pseudopotential, which sometimes is different from the real charge density of the core electrons [70]. Instead, we use a superhard norm-conserving pseudopotential, which reproduces the charge density of the core electrons well.

The combination of $S_{ii}(q)$ and $N(q)$ gives the final result of $W(q)$. As shown in Fig. 1(c), $W(q)$ itself displays some ionic features only at very low temperatures. For example, there is a bump around $q = 4$ Å^{-1} for $T = 2.5$ eV, which corresponds to the peak of $S_{ii}(q)$ in Fig. 1(a), as a typical feature of liquids. With the increase of ionic temperature, the ionic feature disappears as a result of the structureless $S_{ii}(q)$ of the gaseous state. In the figure, the $W(q)$'s of $T = 12$ and 18 eV are typical cases for this condition. It is also displayed that excitations of the core electrons greatly reduce $W(q)$ at high temperature, which means that it will be more difficult to detect ionic features when electrons are heated to a very high temperature.

Contributions of $S_1^b(q)$ are displayed in Fig. 1(d). Note that to compare with $W(q)$, $S_1^b(q)$ is divided by the number of ions N_i. At low temperatures ($T < 15$ eV), the value of $S_1^b(q)$ is less than 3% of $W(q)$, as a result of fairly small contributions of $f_n(1 - f_n)$ in Eq. (19). With a further increase of temperature, $S_1^b(q)$ rises rapidly since a number of inner-shell electrons are thermally excited to nearly free-moving high-energy states. Figure 1(d) shows that at $T = 53$ eV, the value of $S_1^b(q)$ can reach about 1/3 of $W(q)$, which suggests that $W(q)$ itself is not enough for the description of elastic scattering features. It should be noted that for hot dense plasmas where inner-shell states are almost empty, the value of $S_1^b(q)$ will decrease according to Eq. (19). However, its relative contribution to $W(q)$ will maintain on almost the same order since $W(q)$ also decreases with temperature increasing.

B. Comparison with experimental measurements

Combining elastic and inelastic features together, one can thus obtain the entire $S(\boldsymbol{q}, \omega)$. A calculated $S(\boldsymbol{q}, \omega)$ of isochorically heated Be is displayed in Fig. 2(a), together with the experimental XRTS spectrum at $q = 4.27$ Å^{-1}. The calculation is performed at $T = 25$ eV with all four electrons. The temperature agrees well with the radiation-hydrodynamic prediction of Glenzer *et al.* [24] and gives the best fit to the measured spectrum. The instrument function is represented by Voigt-type (Gaussian-Lorentzian mixed) peaks [71] with a total width of ∼80 eV, which convolutes with the $S(\boldsymbol{q}, \omega)$ to get the final spectrum. Note that there are two peaks in the light source. Our calculations show that $S_1(q)/N_i$ is 2.58. The overall agreement of the spectrum with experimental measurements is impressive, as shown in Fig. 2(a), considering there are very few movable parameters in the calculation. The temperature dependency of the XRTS spectra is illustrated by the calculation of $T = 53$ eV, where the temperature is taken from a previous calculation based on Chihara's model [24]. Deviations from the $T = 25$ eV spectrum (and also the experimental measurement) are observed on the shoulders of the main peak, where inelastic scattering features are located. Additionally, our calculations show that calculated XRTS curves having a temperature difference of less than 5 eV will be within the fluctuation range of the measured spectra, and thus hardly distinguished in warm dense experiments.

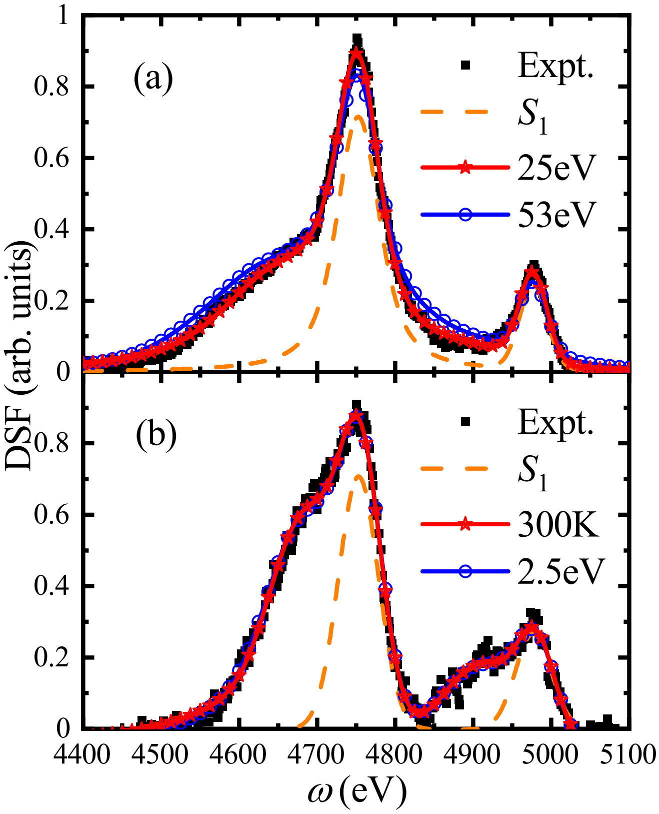

FIG. 2. Calculated $S(\boldsymbol{q}, \omega)$ of Be at transferred momentum $q = 4.27$ Å^{-1} compared with measured spectra [24]. (a) $S(\boldsymbol{q}, \omega)$ calculated at $T = 25$ and 53 eV. The best fit to the measured spectrum of heated Be is at $T = 25$ eV. (b) The calculated $S(\boldsymbol{q}, \omega)$ for crystalline Be at room temperature and $T = 2.5$ eV. Both fit well with the experimental results of cold Be. The elastic contributions convolved with instrument functions are also displayed as orange dashed lines.

Also displayed in Fig. 2(b) are XRTS spectra of cold Be calculated using the same parameters as an example of our method. It shows that the calculation at $T = 300$ K agrees well with the experimental data taken from Glenzer *et al.* [24], which is as expected. In addition, the calculated XRTS spectrum at $T = 2.5$ eV almost coincides with the one at $T = 300$ K, which gives a further estimate of how sensitive the calculated XRTS spectra are under similar thermal conditions in response to the variation of temperature.

V. SUMMARY

In summary, we propose a scheme for predicting the entire XRTS spectrum of WDM based on first-principles methods. A quantum description of XRTS with decomposed expressions of electronic DSF for inhomogeneous systems is presented. The DFT-based FPMD (or ext-FPMD) and the perturbation approach of TDDFT are introduced to address the elastic and inelastic parts separately. This method is then applied to XRTS experiments of isochorically heated Be. Remarkable agreements between calculations and experimental measurements are observed, which implies that this method may bring substantial improvements to the XRTS diagnostics over empirical modeling methods in the future.

ACKNOWLEDGMENTS

This work is financially supported by the National Key Research and Development Program of China (Grant No. 2017YFA0403200), the Science Challenging Project (Grant No. TZ2016001), the NSAF (Grant No. U1530258), and the NSFC (Grant No. 11275032). Part of the calculations are supported by the Special Program for Applied Research on Super Computation of the NSFC-Guangdong Joint Fund (the second phase) under Grant No. U1501501. Z.-G.F. was supported by the National Natural Science Foundation of China (NSFC) under Grant No. 11675023, the Innovation Development Fund of China Academy of Engineering Physics (CAEP) under Grant No. ZYCX1921-02, and the President Foundation of CAEP under Grant No. YZ2015014. C.M. was supported by the NSFC under Grants No. U1930402 and No. 11947202, and by the China Postdoctoral Science Foundation under Grant No. 2019M660016.

[1] J. Lindl, Phys. Plasmas **2**, 3933 (1995).

[2] X. T. He, J. W. Li, Z. F. Fan, L. F. Wang, J. Liu, K. Lan, J. F. Wu, and W. H. Ye, Phys. Plasmas **23**, 082706 (2016).

[3] S. E. Bodner, D. G. Colombant, J. H. Gardner, R. H. Lehmberg, S. P. Obenschain, L. Phillips, A. J. Schmitt, J. D. Sethian, R. L. McCrory, W. Seka, C. P. Verdon, J. P. Knauer, B. B. Afeyan, and H. T. Powell, Phys. Plasmas **5**, 1901 (1998).

[4] E. Campbell, V. Goncharov, T. Sangster, S. Regan, P. Radha, R. Betti, J. Myatt, D. Froula, M. Rosenberg, I. Igumenshchev, W. Seka, A. Solodov, A. Maximov, J. Marozas, T. Collins, D. Turnbull, F. Marshall, A. Shvydky, J. Knauer, R. McCrory, A. Sefkow, M. Hohenberger, P. Michel, T. Chapman, L. Masse, C. Goyon, S. Ross, J. Bates, M. Karasik, J. Oh, J. Weaver, A. Schmitt, K. Obenschain, S. Obenschain, S. Reyes, and B. Van Wonterghem, Matter Radiat. Extremes **2**, 37 (2017).

[5] I. Hofmann, Matter Radiat. Extremes **3**, 1 (2018).

[6] T. Guillot, Science **286**, 72 (1999).

[7] B. A. Remington, R. P. Drake, and D. D. Ryutov, Rev. Mod. Phys. **78**, 755 (2006).

[8] J. E. Miller, T. R. Boehly, A. Melchior, D. D. Meyerhofer, P. M. Celliers, J. H. Eggert, D. G. Hicks, C. M. Sorce, J. A. Oertel, and P. M. Emmel, Rev. Sci. Instrum. **78**, 034903 (2007).

[9] C. Zhang, H. Liu, Z. Wang, X. Jiang, H. Zhang, Y. Liu, Z. Li, S. Li, D. Yang, Y. Ding, B. Zhao, G. Hu, and J. Zheng, Plasma Sci. Technol. **16**, 571 (2014).

[10] Y. Zhao, J. Yang, J. Zhang, G. Yang, M. Wei, G. Xiong, T. Song, Z. Zhang, L. Bao, B. Deng, Y. Li, X. He, C. Li, Y. Mei, R. Yu, S. Jiang, S. Liu, Y. Ding, and B. Zhang, Phys. Rev. Lett. **111**, 155003 (2013).

[11] S. Zhang, S. Zhao, W. Kang, P. Zhang, and X.-T. He, Phys. Rev. B **93**, 115114 (2016).

[12] A. Benuzzi-Mounaix, F. Dorchies, V. Recoules, F. Festa, O. Peyrusse, A. Levy, A. Ravasio, T. Hall, M. Koenig, N. Amadou, E. Brambrink, and S. Mazevet, Phys. Rev. Lett. **107**, 165006 (2011).

[13] S. Vinko, O. Ciricosta, B. Cho, K. Engelhorn, H.-K. Chung, C. Brown, T. Burian, J. Chalupský, R. Falcone, C. Graves *et al.*, Nature (London) **482**, 59 (2012).

[14] S. H. Glenzer and R. Redmer, Rev. Mod. Phys. **81**, 1625 (2009).

[15] Y. Ding, A. Brachmann, F.-J. Decker, D. Dowell, P. Emma, J. Frisch, S. Gilevich, G. Hays, P. Hering, Z. Huang, R. Iverson, H. Loos, A. Miahnahri, H.-D. Nuhn, D. Ratner, J. Turner, J. Welch, W. White, and J. Wu, Phys. Rev. Lett. **102**, 254801 (2009).

[16] J. M. Soures, S. J. Loucks, R. L. McCrory, C. P. Verdon, A. Babushkin, R. E. Bahr, T. R. Boehly, R. Boni, D. K. Bradley, D. L. Brown, J. A. Delettrez, R. S. Craxton, W. R. Donaldson, R. Epstein, R. Gram, D. R. Harding, P. A. Jaanimagi, S. D. Jacobs, K. Kearney, R. L. Keck, J. H. Kelly, T. J. Kessler, R. L. Kremens, J. P. Knauer, S. A. Letzring, D. J. Lonobile, L. D. Lund, F. J. Marshall, P. W. McKenty, D. D. Meyerhofer, S. F. B. Morse, A. Okishev, S. Papernov, G. Pien, W. Seka, R. W. Short, M. D. Skeldon, S. Skupsky, A. W. Schmid, D. J. Smith, S. Swales, M. Wittman, B. Yaakobi, and M. J. Soup III, Fusion Technol. **30**, 492 (1996).

[17] X. T. He and W. Y. Zhang, Eur. Phys. J. D **44**, 227 (2007).

[18] S. Weber, S. Bechet, S. Borneis, L. Brabec, M. Bučka, E. Chacon-Golcher, M. Ciappina, M. DeMarco, A. Fajstavr, K. Falk, E.-R. Garcia, J. Grosz, Y.-J. Gu, J.-C. Hernandez, M. Holec, P. Janečka, M. Jantač, M. Jirka, H. Kadlecova, D. Khikhlukha, O. Klimo, G. Korn, D. Kramer, D. Kumar, T. Lastovička, P. Lutoslawski, L. Morejon, V. Olšovcová, M. Rajdl, O. Renner, B. Rus, S. Singh, M. Šmid, M. Sokol, R. Versaci, R. Vrána, M. Vranic, J. Vyskočil, A. Wolf, and Q. Yu, Matter Radiat. Extremes **2**, 149 (2017).

[19] H. J. Lee, P. Neumayer, J. Castor, T. Döppner, R. W. Falcone, C. Fortmann, B. A. Hammel, A. L. Kritcher, O. L. Landen, R. W. Lee, D. D. Meyerhofer, D. H. Munro, R. Redmer, S. P. Regan, S. Weber, and S. H. Glenzer, Phys. Rev. Lett. **102**, 115001 (2009).

[20] L. Fletcher, H. Lee, T. Döppner, E. Galtier, B. Nagler, P. Heimann, C. Fortmann, S. LePape, T. Ma, M. Millot *et al.*, Nat. Photon. **9**, 274 (2015).

[21] J. Chihara, J. Phys. F **17**, 295 (1987).

[22] J. Chihara, J. Phys.: Condens. Matter **12**, 231 (2000).

[23] G. Gregori, S. H. Glenzer, W. Rozmus, R. W. Lee, and O. L. Landen, Phys. Rev. E **67**, 026412 (2003).

[24] S. H. Glenzer, G. Gregori, R. W. Lee, F. J. Rogers, S. W. Pollaine, and O. L. Landen, Phys. Rev. Lett. **90**, 175002 (2003).

[25] W. Schülke, *Electron Dynamics by Inelastic X-Ray Scattering* (Oxford University Press, Oxford, 2007).

[26] J. Sheffield, *Plasma Scattering of Electromagnetic Radiation* (Academic Press, New York, 1975).

[27] H. Reinholz, Ann. Phys. Fr. **30**, 1 (2005).

[28] M. D. Barriga-Carrasco, Phys. Rev. E **79**, 027401 (2009).

[29] C. Fortmann, A. Wierling, and G. Röpke, Phys. Rev. E **81**, 026405 (2010).

[30] Z.-G. Fu, Z. Wang, M.-L. Li, D.-F. Li, W. Kang, and P. Zhang, Phys. Rev. E **94**, 063203 (2016).

[31] Z.-G. Fu, Z. Wang, C. Mo, D. Li, W. Li, Y. Lu, W. Kang, X.-T. He, and P. Zhang, Phys. Rev. E **101**, 053209 (2020).

[32] H. R. Rüter and R. Redmer, Phys. Rev. Lett. **112**, 145007 (2014).

[33] K.-U. Plagemann, H. R. Rüter, T. Bornath, M. Shihab, M. P. Desjarlais, C. Fortmann, S. H. Glenzer, and R. Redmer, Phys. Rev. E **92**, 013103 (2015).

[34] J. Vorberger and D. O. Gericke, Phys. Rev. E **91**, 033112 (2015).

[35] C. Mo, Z. Fu, W. Kang, P. Zhang, and X. T. He, Phys. Rev. Lett. **120**, 205002 (2018).

[36] T. Dornheim, S. Groth, J. Vorberger, and M. Bonitz, Phys. Rev. Lett. **121**, 255001 (2018).

[37] K. Ramakrishna and J. Vorberger, J. Phys.: Condens. Matter **32**, 095401 (2019).

[38] K.-U. Plagemann, P. Sperling, R. Thiele, M. P. Desjarlais, C. Fortmann, T. Döppner, H. J. Lee, S. H. Glenzer, and R. Redmer, New J. Phys. **14**, 055020 (2012).

[39] A. D. Baczewski, L. Shulenburger, M. P. Desjarlais, S. B. Hansen, and R. J. Magyar, Phys. Rev. Lett. **116**, 115004 (2016).

[40] B. B. L. Witte, M. Shihab, S. H. Glenzer, and R. Redmer, Phys. Rev. B **95**, 144105 (2017).

[41] B. B. L. Witte, P. Sperling, M. French, V. Recoules, S. H. Glenzer, and R. Redmer, Phys. Plasmas **25**, 056901 (2018).

[42] D. Pines and P. Nozières, *The Theory of Quantum Liquids*, Vol. 1 (Benjamin, New York, 1966).

[43] P. Sperling, E. J. Gamboa, H. J. Lee, H. K. Chung, E. Galtier, Y. Omarbakiyeva, H. Reinholz, G. Röpke, U. Zastrau, J. Hastings, L. B. Fletcher, and S. H. Glenzer, Phys. Rev. Lett. **115**, 115001 (2015).

[44] L. B. Fletcher, E. Galtier, P. Heimann, H. J. Lee, B. Nagler, J. Welch, U. Zastrau, J. B. Hastings, and S. H. Glenzer, J. Instrum. **8**, C11014 (2013).

[45] S. P. Hau-Riege, A. Graf, T. Döppner, R. A. London, J. Krzywinski, C. Fortmann, S. H. Glenzer, M. Frank, K. Sokolowski-Tinten, M. Messerschmidt, C. Bostedt, S. Schorb, J. A. Bradley, A. Lutman, D. Rolles, A. Rudenko, and B. Rudek, Phys. Rev. Lett. **108**, 217402 (2012).

[46] J. Vorberger and D. A. Chapman, Phys. Rev. E **97**, 013203 (2018).

[47] R. M. Martin, *Electronic Structure: Basic Theory and Practical Methods* (Cambridge University Press, Cambridge, 2004).

[48] S. Zhang, H. Wang, W. Kang, P. Zhang, and X. T. He, Phys. Plasmas **23**, 042707 (2016).

[49] C. Gao, S. Zhang, W. Kang, C. Wang, P. Zhang, and X. T. He, Phys. Rev. B **94**, 205115 (2016).

[50] D. Kraus, J. Vorberger, D. O. Gericke, V. Bagnoud, A. Blažević, W. Cayzac, A. Frank, G. Gregori, A. Ortner, A. Otten, F. Roth, G. Schaumann, D. Schumacher, K. Siegenthaler, F. Wagner, K. Wünsch, and M. Roth, Phys. Rev. Lett. **111**, 255501 (2013).

[51] M. Lv, Z. Hu, Y. Hou, M. Wei, C. Mo, W. Zheng, M. Lv, G. Yang, Y. Zhao, Z. Zhang, B. Qing, G. Xiong, X. Zhan, L. Hou, W. Zhang, W. Kang, P. Zhang, J. Yuan, J. Zhang, and J. Yang, Phys. Plasmas **26**, 022702 (2019).

[52] M. Petersilka, U. J. Gossmann, and E. K. U. Gross, Phys. Rev. Lett. **76**, 1212 (1996).

[53] L. D. Landau and E. M. Lifshitz, *Statistical Physics, Part 1 (Course of Theoretical Physics, Vol. 5)*, 3rd ed. (Pergamon Press, Oxford, 1980).

[54] G. Onida, L. Reining, and A. Rubio, Rev. Mod. Phys. **74**, 601 (2002).

[55] P. Giannozzi, S. Baroni, N. Bonini, M. Calandra, R. Car, C. Cavazzoni, D. Ceresoli, G. L. Chiarotti, M. Cococcioni, I. Dabo, A. D. Corso, S. de Gironcoli, S. Fabris, G. Fratesi, R. Gebauer, U. Gerstmann, C. Gougoussis, A. Kokalj, M. Lazzeri, L. Martin-Samos, N. Marzari, F. Mauri, R. Mazzarello, S. Paolini, A. Pasquarello, L. Paulatto, C. Sbraccia, S. Scandolo, G. Sclauzero, A. P. Seitsonen, A. Smogunov, P. Umari, and R. M. Wentzcovitch, J. Phys.: Condens. Matter **21**, 395502 (2009).

[56] P. E. Blöchl, Phys. Rev. B **50**, 17953 (1994).

[57] J. P. Perdew, K. Burke, and M. Ernzerhof, Phys. Rev. Lett. **77**, 3865 (1996).

[58] R. Elmer, M. Berg, L. Carlen, B. Jakobsson, B. Noren, A. Oskarsson, G. Ericsson, J. Julien, T. F. Thorsteinsen, M. Guttormsen, G. Lovhoiden, V. Bellini, E. Grosse, C. Muntz, P. Senger, and L. Westerberg, Phys. Rev. Lett. **78**, 1396(E) (1997).

[59] D. R. Hamann, M. Schlüter, and C. Chiang, Phys. Rev. Lett. **43**, 1494 (1979).

[60] A. Marini, C. Hogan, M. Grüning, and D. Varsano, Comput. Phys. Commun. **180**, 1392 (2009).

[61] D. Sangalli, A. Ferretti, H. Miranda, C. Attaccalite, I. Marri, E. Cannuccia, P. Melo, M. Marsili, F. Paleari, A. Marrazzo, G. Prandini, P. Bonfà, M. O. Atambo, F. Affinito, M. Palummo, A. Molina-Sánchez, C. Hogan, M. Grüning, D. Varsano, and A. Marini, J. Phys.: Condens. Matter **31**, 325902 (2019).

[62] I. Timrov, N. Vast, R. Gebauer, and S. Baroni, Phys. Rev. B **88**, 064301 (2013).

[63] E. W. Brown, B. K. Clark, J. L. DuBois, and D. M. Ceperley, Phys. Rev. Lett. **110**, 146405 (2013).

[64] V. V. Karasiev, T. Sjostrom, J. Dufty, and S. B. Trickey, Phys. Rev. Lett. **112**, 076403 (2014).

[65] V. V. Karasiev, L. Calderín, and S. B. Trickey, Phys. Rev. E **93**, 063207 (2016).

[66] S. H. Glenzer, O. L. Landen, P. Neumayer, R. W. Lee, K. Widmann, S. W. Pollaine, R. J. Wallace, G. Gregori, A. Höll, T. Bornath, R. Thiele, V. Schwarz, W.-D. Kraeft, and R. Redmer, Phys. Rev. Lett. **98**, 065002 (2007).

[67] T. Döppner, O. Landen, H. Lee, P. Neumayer, S. Regan, and S. Glenzer, High Energy Density Phys. **5**, 182 (2009).

[68] K. Wünsch, J. Vorberger, and D. O. Gericke, Phys. Rev. E **79**, 010201(R) (2009).

[69] R. A. Valenza and G. T. Seidler, Phys. Rev. B **93**, 115135 (2016).

[70] N. Holzwarth, A. Tackett, and G. Matthews, Comput. Phys. Commun. **135**, 329 (2001).

[71] G. D. Roston and F. S. Obaid, J. Quantum Spectrosc. Radiat. Transfer **94**, 255 (2005).